Potential of Waste Oyster Shells as a Novel Biofiller for Hot-Mix Asphalt

Nader Nciri, Taesub Shin, Haksoo Lee and Namjun Cho *

Department of Energy, Materials, and Chemical Engineering, Korea University of Technology and Education, 1600 Chungjeol-ro, Byeongcheon-myeon, Dongnam-gu, Cheonan-City, Chungnam-Province 330-708, Korea; nader.nciri@koreatech.ac.kr (N.N.); teaja21@koreatech.ac.kr (T.S.); haktop10@koreatech.ac.kr (H.L.)
* Correspondence: njuncho@koreatech.ac.kr; Tel.: +82-41-560-1342

Abstract: This paper reports the use of waste oyster shells as a novel biofiller for hot-mix asphalt (HMA) pavement applications. The effects of different fractions (e.g., 0, 5, 10, 15 wt %) of oyster shell powder (OSP) on the bitumen performance were investigated. The chemical properties of unfilled and OSP-filled asphalts were characterized by means of thin layer chromatography-ionization detection (TLC-FID), Fourier transform-infrared spectroscopy (FT-IR), X-ray diffraction (XRD), and scanning electron microscopy (SEM). Thermal characteristics were examined by thermogravimetric analysis (TGA) and differential scanning calorimetry (DSC). Physical and rheological properties were assessed through penetration, softening point, ductility, and dynamic shear rheometer (DSR) tests. Results showed that OSP addition increased the resins content, as well as the stiffness of blends. No obvious reactions have occurred between the filler and the asphalt. A higher dose of OSP altered the morphology of the binder, whereas lower and intermediate doses improved its thermal stability and enhanced its low-temperature, rutting, and fatigue performances with respect to the plain asphalt. Overall, the waste oyster shells could be used as filler substitute, not only to improve the quality of road pavements but also to reduce the cost of their construction and solve the waste disposal problems.

Keywords: oyster shell powder; calcite filler; asphalt mastics; rutting; fatigue cracking; thermal stability; glass transition temperature

1. Introduction

Hot-mix asphalt (HMA) is a heterogeneous multiphase material that consists of aggregates with different sizes and shapes, asphalt cement, and air voids. These components constitute a complex microstructure. While the aggregates act basically as a skeleton, asphalt binder provides an adhesive action (i.e., glue) among aggregate particles and contributes to the viscous-elastic properties of the mixture [1]. Aggregates in HMA can be divided into three types according to their size: coarse aggregates, fine aggregates, and mineral filler. Coarse aggregates are generally defined as those retained on the 2.36-mm sieve. Fine aggregates are those that pass through the 2.36-mm sieve and are retained on the 0.075-mm sieve. Mineral filler is defined as that portion of the aggregate passing the 0.075-mm sieve [2].

Mineral filler is a very fine material with the consistency of flour and is also referred to as mineral dust or rock dust. It can greatly affect the properties of a mixture such as strength, plasticity, voids, resistance to action of water, and the resistance to the forces of weathering. The proper use of filler can improve the asphalt paving mixture through increased density, stability, durability, and skid resistance. On the other hand, excessive quantity of filler tends to increase brittleness and proclivity to cracking, and deficiency of filler tends to increase void content, lower stability, and soften the mix,

which leads to shoving, and rutting of the pavement [3]. Mineral fillers play a dual role in paving mixtures. First, they are part of the mineral aggregate, i.e., they fill the interstices and provide contact points between larger aggregate particles and, thereby, strengthen the mixture. Second, when mixed with asphalt, mineral fillers form a high-consistency binder or matrix that cements larger aggregate particles together. This resulting filler-asphalt mastic is capable of affecting the physical and mechanical properties of the mixture to a large extent [4].

Various studies have shown that there are three primary mechanisms by which fillers reinforce asphalt binder [5–7]: volume filling, particle struturalization, and physicochemical interactions. Volume filling and particle struturalization are both means of mechanical reinforcement. Volume filling increases asphalt mastic stiffness simply as a result of the replacement of asphalt binder volume with rigid particles. Filler particles start to form an interconnected network at a filler volumetric concentration of roughly 40%, leading to a rapid increase in the rate of stiffening with increasing volume fraction [6,8,9]. At lower filler concentrations, particle contact is not established, and the mastic will behave as a dilute suspension, with volume filling constituting the dominant mechanical reinforcement mechanism. The third type of reinforcement, physico-chemical interaction, involves the adsorption of polar fractions (e.g., resins and asphaltenes) of the asphalt binder onto the surface of filler particles through electrostatic, dipole–dipole, or van der Waals forces [7,10,11]. Physiochemical interaction leads to the formation of an interphase adsorbed layer of the polar fractions of asphalt on the surface of filler particles. In addition, loss of certain components of the asphalt to adsorption modifies the chemistry and morphology of the non-adsorbed, "effective" binder matrix [12].

Different types of filler including limestone dust, Portland cement, crushed stone, granite powder, and fine sand are usually used in the asphalt mixtures [3]. Society's ever-growing concern for protecting the environment has resulted in concentrated attention on the possible reuse of waste materials in road construction [13–17]. Numerous efforts have been made to use waste materials of various origins to partially or fully replace conventional filler in the production of HMA. The wastes that were identified included construction and demolition waste (e.g., crushed bricks and concrete) [18], marble slurry [19], coal waste powder [20], waste glass [21], rice husk ash [22], coconut shells [23], eggshells [24], and seashells [25], etc. It has been found that these materials contain recoverable fractions that are potentially useful in highway related applications. There are numerous examples of successful applications in highway construction for each of these materials. By removing these materials from the waste stream and recycling them in highway applications, demand for virgin raw materials will be reduced, street and highway maintenance costs will be lowered, energy consumption will be reduced, and valuable landfill space will be conserved.

The southeastern coastal sea of South Korea has long been considered one of the most productive oyster growing areas in the world. Shellfish farming makes up a large portion of the local economy. It is estimated that approximately 300,000 tons of oyster shells are produced annually from the shellfish farms, which cover 4100 ha of coastal ocean [26]. The oyster constitutes one of the primary products of shellfish farms, and its industries have greatly contributed to the economic growth, at both national and regional levels [27]. However, disposal of oyster shell waste (OSW) is becoming an increasingly serious problem for the marine aquaculture industry. Huge amounts of OSW are being dumped illegally and constantly into public waters and reclaimed lands, causing a nasty smell as a consequence of the decay of flesh remnants that are attached to the oysters [28]. In an attempt to solve this issue, the government of the Republic of Korea has implemented specific programs and policies to maximize reuse, recycling, and waste reduction [29]. For instances, 10% of OSW is currently recycled as shell meal fertilizer and 50% as catching materials for oyster seedlings (i.e., oyster shells for growing oyster). Unfortunately, and despite all the state efforts made, the remaining part (i.e., 40%) of the OSW is directly dumped in the coastal region, causing environmental problems including pollution of coastal fisheries, the management problem of public water surface, damage of natural landscape, and health/sanitation problems [30]. To cope with this critical situation, new and alternative approaches for recycling OSWs must urgently be found. The ideal solution would be to convert the calcium carbonate-rich OSW to a product that is both beneficial and economically viable.

The purpose of this preliminary investigation was then to assess, for the first time, the feasibility of using OSW as a performance-enhancing additive for road paving applications. It was undertaken to assist those who have an interest in using or increasing their understanding of the oyster shell materials that may be recovered and used in pavement construction applications. It is intended to provide the potential user or reviewer with sufficient information on the use of oyster shell waste so that he will gain a deeper understanding of the material nature and properties, where other information may be obtained, and what issues need to be evaluated when considering its use in hot-mix asphalt (HMA). However, this research article does not constitute a standard, specification, or regulation.

2. Materials and Methods

2.1. Preparation of Oyster Shell Powder (OSP)

Specimens of the *Crassostrea gigas* (Figure 1A) were collected from Tongyeong beach, Gyeongsang province, South Korea. First, the oyster shells were properly cleaned by brushes after discarding the fresh remnant to them. Subsequently, they were well washed with deionized water (DI water) to remove the excess of alkalinity and chloride, and dried in a drying oven ($T = 100$ °C) for ca. 2 days. The dried shells were ground (4 times, 4 hours per round) using a dry ball-mill (Oyster Shell Grinding Machine, Zhengzhou Jiangtai Heavy Industrial Machinery Co., Ltd, Weihai, China) to generate a fine powder, which was then sieved in a No. 50 sieve (300 μm). In practical applications, fillers with a granulometry of less than 75 μm (i.e., passing ASTM standard sieve No. 200) are used to provide the best homogenous asphalt mixtures [31]. However, the asphalt pavement design may not be the greatest scenario for maximizing pavement performance when pavement distresses such as fatigue cracking, rutting, and moisture damage occur. Therefore, the purpose of this investigation was to determine the influence and effects of a wide range of different particle sizes (up to 300 μm) on the asphalt-filler mastic performance properties through selected Superpave (i.e., Superior Performance Asphalt Pavement) binder tests. It must be emphasized here that this was done only to learn about the advantages and disadvantages associated with the use of particles larger than the standard. Hence, the aforementioned procedure is not intended to be used in practice. After sieving, the oyster shell powder (labelled as OSP, Figure 1B) was stored at room temperature in a closed container. The particle size and distribution of OSP were performed using a Mastersizer 3000 Smarter Particle Sizing (Malvern Instruments Ltd., Malvern, UK) granulometer. The measurement was carried out at room temperature (ca. 25 °C) with an Aero S dry powder disperser ($P = 1$ bar). The chemical composition was conducted using elemental analyzer (Thermo Scientific™ FLASH 2000 CHNS/O Analyzer, Loughborough, UK), X-ray fluorescence spectrometer (Shimadzu EX-720, Shimadzu Corporation, Chiyoda-ku, Tokyo, Japan), and energy-dispersive spectroscopy (SEM, JSM-6010LA, JEOL Ltd., Akishima, Tokyo, Japan).

Figure 1. Oyster shell waste (**A**) and its fine powder (**B**).

2.2. Preparation of Filler-Asphalt Mastic Samples

One-base bitumen, denoted as AP-5 asphalt (penetration grading of 60–70 at 25 °C), was used in this study. It was obtained from SK Energy Co. Ltd. Seoul, Republic of Korea. The physicochemical properties of AP-5 asphalt are given in Table 1. The mastics were produced following a standardized experimental protocol, optimized in order to obtain homogeneous OSP-asphalt mastics. The samples were prepared using a high shear L5M-A mixer (Silverson Machines Inc., East Longmeadow, MA, USA) at 180 °C and a speed of 3000 rpm. The OSP contents used were 5, 10, 15 wt % by weight of blend. These percentages were chosen to see closely the impact of a gradual increase in OSP concentration on the attributes of asphalt cement. In preparation, 600 g of the asphalt heated to fluid condition was poured into a 1000 mL stainless steel container. Upon reaching 175 °C, a preweighed amount of OSP was slowly added to the binder in small quantities of approximately half teaspoon. This was done to ease smooth mixing and prevent agglomeration of the additive. The filler also was introduced into the binder about 2.5 cm above the surface of the bitumen, so that the finest part of the filler would not be lost into the air. Mixing was then continued at 180 °C for 2 hours to ensure good distribution and dispersion of filler particles. Due to the fact that the preparation procedure will lead to the oxidation of asphalt and changes in its properties, it was also applied on the plain bitumen to achieve the same effect.

After completion, the asphaltic sample was removed from the can and divided into small containers. The blend was cooled to room temperature, sealed with aluminum foil, and stored in a dark chamber thermostated at 25 °C to retain the obtained morphology. Since pretreatment introduces additional cost, the waste of oyster shell powder was intactly mixed with the binder without any prior treatment. This also allows one to study solely the direct effects of filler on the bitumen performance.

Table 1. Chemical and physical properties of AP-5 asphalt (PG/60–70).

Elemental Analysis	
C (carbon)	84.62 wt %
H (hydrogen)	10.39 wt %
N (nitrogen)	0.65 wt %
S (sulfur)	3.69 wt %
O (oxygen)	0.65 wt %
SARA Generic Fractions	
Saturates	4.47 wt %
Aromatics	17.45 wt %
Resins	45.18 wt %
Asphaltenes	32.90 wt %
Physical Properties	
Penetration at 25 °C	60.00 dmm
Softening point	50.00 °C
Ductility at 25 °C	110.50 cm

2.3. Fourier Transform-Infrared Spectroscopy (FT-IR)

A HYPERION 3000 FT-IR Spectrometer (Bruker Optics, Ettlingen, Germany) was employed to determine whether there were new functional groups that had been generated through OSP additions. The specimen was prepared with the thin KBr disk method. The asphaltic samples were scanned at 32 times with test range from 400 to 4000 cm^{-1}. All samples were scanned in duplicate.

2.4. X-ray Diffraction (XRD)

The XRD data collection was carried out by a Bruker AXS D8 Advance Diffractometer (Bruker AXS GmbH D8 Advance, Karlsruhe, Germany) employing CuKα radiation (λ = 1.54055 Å). The X-ray generator voltage and current were held at 40 kV and 40 mA, respectively. OSP and

asphaltaneous samples were scanned, at room temperature (ca. 25 °C), from 5° to 100° in 2θ range with 0.020° step size and 2 seconds step^{-1} counter-time. Ten (10) consecutive measurements were performed and added to each other to increase peak intensities and reduce the signal to noise ratio. A very broad peak between 13° and 30° and a small hump around 42° were detected in X-ray diffractograms of bituminous samples.

2.5. Thin-Layer Chromatography-Flame Ionization Detection (TLC-FID)

Thin-layer chromatography-flame ionization detection (TLC-FID or Iatroscan) allows for the fractionation of asphalt into four generic fractions, namely, saturates, aromatics, resins, and asphaltenes (SARA) [32]. Chemical compositions of the base asphalt and OSP-filled asphalts were measured by the MK-6 analyzer (Iatron Laboratories Inc., Tokyo, Japan). Sample solutions with concentration of 2% (m/v) were prepared by dissolving 80 mg sample in 4 mL dichloromethane. Afterwards, the chromarods were cleaned and activated in FID-flame; 1 μL of the solution was spotted on the chromarod using a spotter. The separation of asphalt binder fractions was performed with a three-stage process. The first development was in *n*-hexane (60 mL) and expanded to 100 mm of the chromarods, the second stage in toluene (60 mL) was developed to 70 mm, and the last development was in mixture of dichloromethane/methanol (60 mL, 95/5 by volume) and expanded to 35 mm. The chromarod was dried at 50 °C for 10 min after each development. Then, the chromarods were scanned in the TLC-FID analyzer. A scan rate of 30 s scan^{-1} was used. Air and hydrogen flows were 2000 mL min^{-1} and 160 mL min^{-1}, respectively. SARA analysis was repeated five times at least to ensure reproducibility and accuracy of the results.

2.6. Scanning Electron Microscope (SEM)

The rheological examination was associated with a morphological characterization of asphalt samples, which was conducted by using a Scanning Electron Microscope (JSM-6010LA, JEOL Ltd., Tokyo, Japan). The evaluation was aimed principally at estimating the distribution of OSP particles in the bituminous matrix and determining possible relationships between the microstructure and rheological performance. The analysis was carried out on the surface of samples (ca. 8 mm width and 2 mm thickness). Since the bitumen is nonconductive material, its surface was metalized by applying a thin coating of gold before starting SEM analysis. The images were then scanned in backscattered electron mode with an acceleration tension of electronic beam equal to 5 kV. This was done to prevent irreversible thermal damage to the sample surface. The specimens were photographed at different magnifications (e.g., ×500 and ×3000).

2.7. Thermogravimetric Analysis (TGA/DTGA)

The weight loss of OSP, and untreated and OSP-treated asphalt samples, was monitored by thermogravimetric analysis (TGA) using a TA Instruments TGA Q500 thermogravimetric analyzer (TA Instruments, New Castle, DE, USA). Briefly, a piece of approximately 15–20 mg of specimen was cut out and placed in platinum crucible. The analyses were carried out at temperatures between room temperature (ca. 25 °C) and 1000 °C using a nitrogen gas flow of 150 mL min^{-1}. The scanning rate was 10 °C min^{-1}. Thermogravimetric parameters such as the temperature of initial weight loss (T_{onset}), temperature of final weight loss (T_{offset}), temperature of maximum rate of weight loss (T_{max}), and carbonaceous residue at 1000 °C (ΔW, wt %) were determined from the TGA and DTGA curves. All TGA tests were run in triplicate to ensure reproducibility and accuracy.

2.8. Differential Scanning Calorimetry (DSC)

The DSC heat flow as a function of temperature curves was measured for asphalt using a Perkin-Elmer DSC 8000 (PerkinElmer Inc., Waltham, MA, USA) and for oyster shell powder (OSP) using a NETZSCH Simultaneous Thermal Analyzer (STA) 449 F5 Jupiter® (NETZSCH-Gerätebau GmbH, Wittelsbacherstraße, Germany). OSP samples of approximately 10–15 mg were held in DSC-TGA Alumina (Al$_2$O$_3$) crucibles at the heating rate of 10 K min^{-1} under an argon flow rate of 50 mL min^{-1}

at temperatures ranging from 28 °C to 1000 °C. To perform DSC scans for bituminous specimens, approximately 15–20 mg of base asphalt or OSP-filled asphalt was transferred to a hermetically sealed pan. The pan containing the sample was then placed in the DSC apparatus and maintained at 50 °C for 10 min. Subsequently, the sample was rapidly cooled down to −90 °C at a cooling rate of 20 °C min^{-1} followed by a heating from −90 °C to 150 °C. This cooling and heating cycle was executed to eliminate the thermal history of asphalt sample. Finally, the sample was cooled down to −90 °C, held at this temperature for 10 min, then heated to 150 °C at a heating rate of 20 °C min^{-1}. DSC heat flow as a function of temperature data was recorded during the heating process of the second cycle. In this work, DSC test was undertaken to determine the glass transition temperature (T_{g1}) of the unfilled and OSP-filled asphalts. Each DSC test was repeated three times at least, to ensure the reproducibility and accuracy of results.

2.9. Conventional Asphalt Binder Tests (Penetration, Softening Point, and Ductility)

The physical properties of unfilled and OSP-filled asphalts were evaluated by different empirical tests including softening point, ductility, and penetration. The softening point of binder was determined in accordance with ASTM D36 [33], while the ductility was conducted in accordance with ASTM D113 standard [34]. The penetration test, which indicates the binder hardness, was performed in accordance with ASTM D5 [35]. The penetration index (PI) is considered as a measure of temperature susceptibility of asphalt cement. The temperature susceptibility of bituminous samples was calculated using the results obtained from penetration and softening point tests as follows [36,37]:

$$PI = \frac{1952 - 500 \log (Pen\ 25) - 20 \times SP}{50 \log (Pen25) - SP - 120} \tag{1}$$

in which Pen 25 is the penetration at 25 °C (dmm) and SP is the softening point (°C) of bitumen sample. The PI values vary usually from −3 for high temperature susceptible asphalts to about +7 for highly blown low temperature susceptible asphalt [1]. Each experiment was repeated three times independently, to ensure the reproducibility and accuracy of results.

2.10. Dynamic Shear Rheometer (DSR)

A dynamic shear rheometer (DSR, MCR101, Anton Paar Company, Virginia, USA) was used to measure the rheological properties of unfilled and OSP-filled asphalts. DSR test was conducted in accordance with ASTM D7175-15 [38]. The rutting and fatigue cracking performances of bitumen specimens were assessed through $G^*/\sin \delta$ and $G^*.\sin \delta$, respectively. In this research, the test was conducted from 52 °C to 70 °C at an increment of 6 °C for the rutting performance and from 31 to 19 °C at a decrement of 3 °C for the fatigue cracking performance. For the unaged and RTFO- (i.e., rolling thin-film oven) asphalt samples, a 1 mm-thick plate and 25 mm-diameter top plate was employed. On the other hand, a 2 mm-thick plate and 8 mm-diameter top plate was used for PAV- (i.e., pressure aging vessel) binder specimens. The asphalt was sandwiched between two fixed plates. Stress was applied on top of the sample by the oscillating top plate, which oscillated at 1.59 Hz, to measure the maximum stress, maximum strain, and lag of stress and strain. All test results shown in this work represent the average of three replicates.

3. Results

3.1. Chemical Composition of Oyster Shell Powder (OSP)

CHNS/O analysis, X-ray fluorescence (XRF), and energy-dispersive spectroscopy (EDS) were used to find out the precise values of calcium oxide (CaO), carbon (C), and oxygen (O), respectively, in the oyster shell powder (OSP) of *Crassostrea gigas*. The concentration of chemicals as per the test results is given in Table 2 and Figure 2. Calcium oxide was observed as the largest constituent at 99.033 wt % following by total oxygen at 34.023 wt %. Elemental analysis confirmed that shell powder is mainly composed of $CaCO_3$, since the measured carbon content (12.072 wt %) is very close to its

theoretical content (12.000 wt %). The remaining elements are sulfur trioxide (0.518 wt %), strontium oxide (0.311 wt %), and nitrogen (0.189 wt %). Ferric oxide (Fe_2O_3), cupric oxide (CuO), magnesium oxide (MnO), hydrogen (H), and sulfur (S) exist only in minor amounts. The raw material used in this experiment is a highly pure calcite, which is expected to influence the physical and rheological properties of asphalt cement when it is introduced into its matrix [3,4,39,40].

Table 2. Chemical composition of oyster shell powder (OSP) as raw material used in this work.

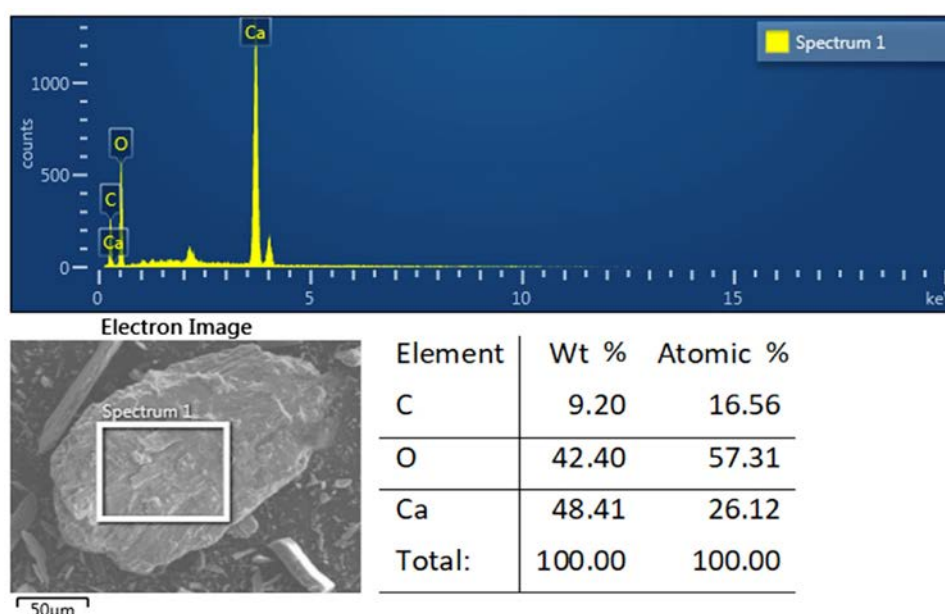| Organic Compounds	Concentration (wt %)
C (carbon)	12.072
H (hydrogen)	0.092
N (nitrogen)	0.189
S (sulfur)	0.000
O (oxygen)	34.023
Total	46.376
Inorganic Compounds	**Percentage (wt %)**
CaO (calcium oxide)	99.033
SO_3 (sulfur trioxide)	0.518
SrO (strontium oxide)	0.311
Fe_2O_3 (ferric oxide)	0.086
CuO (cupric oxide)	0.030
MnO (magnesium oxide)	0.023
Total	100.00

Figure 2. Scanning electron microscopy (SEM) with energy-dispersive spectroscopy (EDS) microanalysis for oyster shell powder (OSP).

3.2. Particle-Size Distribution (PSD) of Oyster Shell Powder (OSP)

Figure 3 portrays a typical particle size distribution (PSD) histogram of oyster shell powder (OSP) obtained with dry ball grinding. As visualized in this Figure, the sample presents large PSD varying mainly between 111 μm and 211 μm, validating the SEM observation (i.e., powder particles with irregular shapes and different sizes). This behavior could largely be attributed to the higher hardness of the shells, because there is a higher content of calcite in the shells that increases the shell hardness and strength. Certain characteristic parameters representative of the distribution curve are summarized in Table 3. The size distribution data obtained from a laser diffraction measurement

shows that Dv (50) is 71.10 μm, which represents 50% of particles that are below 71.10 μm (i.e., the median diameter). Similarly, Dv (10) and Dv (90) are 2.98 μm and 307 μm, indicating that 10% of particles are below 2.98 μm (i.e., fine fraction) and 90% of particles are below 307 μm (i.e., coarse fraction), respectively. It is generally recognized that the small particles have large, specific surface area (SSA) to interact with asphalt matrix and can be homogeneously dispersed in it, and the opposite is also true [41–43]. Usually, the mineral aggregates of road pavements are suspended throughout a mixture and vary in size from coarse to fine. Adequately compacted asphaltic mixtures generate a structure whose stiffness, stability, and wearing characteristics depend on the cohesiveness of the binder and the interlocking of the aggregates particles. Only the fraction of the mineral filler composed of particles thicker than the asphalt film contributes to the aggregate interlocking. The other fraction of the filler, i.e., the fine particles smaller than the thickness of the asphalt film, is distributed in the asphalt phase and is part of the binder component of the mixture [44].
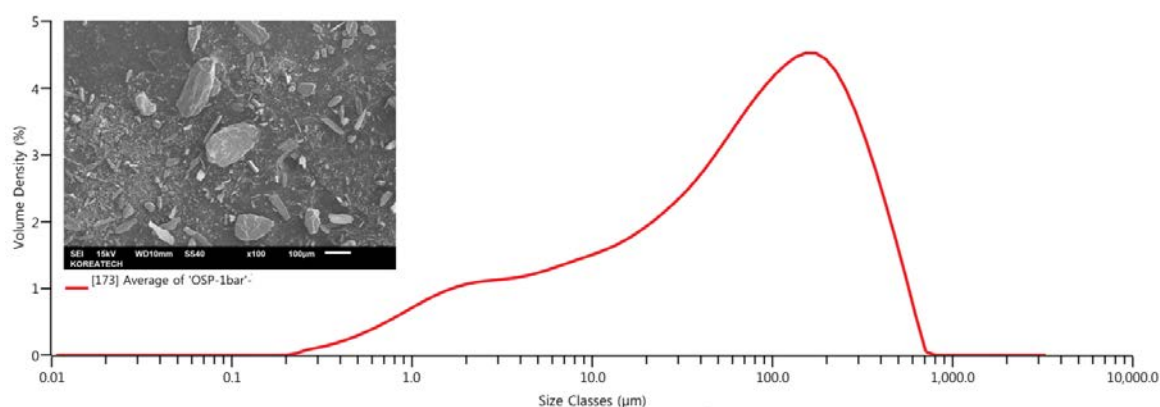

Figure 3. Typical particle size distribution for oyster shell powder (OSP) after dry ball milling process.

Table 3. Particle-size distribution (PSD) data of oyster shell powder (OSP) achieved using a dispersive air pressure 1 bar.

Parameter	Value
Span	4.273 μm
Weighted residual	0.12%
Specific surface area	0.7582 $m^2 \ g^{-1}$
D [3,2]	7.91 μm
D [4,3]	117 μm
Dv (10)	2.98 μm
Dv (50)	71.10 μm
Dv (90)	307 μm
Mode	162 μm

Span = [Dv (90) − Dv (10)]/Dv (50) (μm) represents the width or breadth of the distribution based on the 10%, 50%, and 90% quantile. D represents the diameter of powder particles (μm). D [3,2]: equivalent surface area mean diameter or the Sauter mean diameter (μm). D [4,3]: equivalent volume mean diameter or the De Broncker mean diameter (μm). Dv (10): 10% of the distribution lies below the D10 (μm). Dv (50), D50, or median, defined as a diameter in which half of the population lies below this value (μm). Dv (90): 90% of the distribution lies below the D90 (μm). Mode, size with highest frequency (μm), represents the particle size (or size range) most commonly found in the distribution.

3.3. Fourier Transform-Infrared Spectroscopy (FT-IR)

Possible interactions between the oyster shell powder (OSP) and the bitumen matrix were analyzed using FT-IR spectroscopy. The OSP, base asphalt, and OSP-filled asphalts were examined for this purpose. The FT-IR spectra of OSP, and unfilled and OSP-filled asphalts, are given in Figure

4. As can be seen, all samples are characterized by various bands ranging from 400 to 4000 cm^{-1}. Referring to the IR spectra of plain bitumen (i.e., AP-5 OSP 0 wt %) and filler-asphalt mastics, the absorption bands at 722 cm^{-1} correspond to the rocking vibration of the group (–CH$_2$–CH–)$_n$. The absorption bands at 1376 cm^{-1} are assigned to the symmetric bending vibration of CH$_3$ functional group, whereas, the absorption bands at 1457 cm^{-1} are due to the asymmetric bending vibration of –CH$_3$ groups and the scissor bending vibration of –CH$_2$– groups. The absorption bands at 2851 cm^{-1} and 2921 cm^{-1} result from the symmetric stretching of –CH$_3$ and the asymmetric stretching of –CH$_2$–, respectively. In the OSP spectrum, the small peak located at 1794 cm^{-1} may correspond to the combination vibrations of –NH– *in*-plane bending and C=O stretching. The shoulder of carbonate compounds (e.g., bicarbonate ion, HCO_3^-) occurs at 2513 cm^{-1}. On the other hand, the intensities of the C–O bands of oyster shell powder between 500 cm^{-1} and 1500 cm^{-1} are the strongest. The multiple bands observed at 712, 874, 1159, and 1396 cm^{-1} are ascribed to the *in*-plane bending vibration, the *out*-of-plane bending vibration, the symmetric stretching, and the asymmetric stretching of carbonate ion (i.e., CO_3^{2-}), respectively [45,46]. From the foregoing data, it is evident that no new characteristic absorption bands of OSP/asphalt blends was generated, thereby demonstrating that no chemical reaction took place between the oyster shell powder and the asphalt cement.
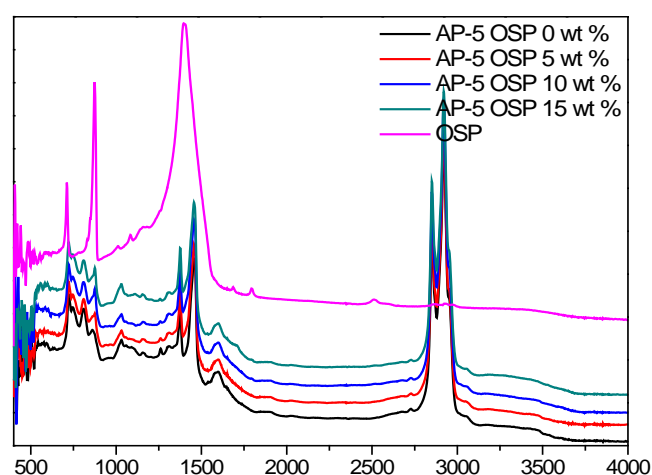

Figure 4. FT-IR spectra of OSP, neat asphalt, and OSP-filled asphalts.

3.4. X-ray Diffraction (XRD)

X-ray diffraction (XRD) patterns of OSP, neat asphalt, and OSP-filled asphalts are shown in Figure 5. Oyster shells are biological wastes, which are mainly made up of calcium carbonate (≥96 wt %) and minor amounts of other minerals. It can clearly be seen that the major crystalline phase of oyster shell waste is calcite (i.e., CaCO$_3$). No peaks due to other phases were detected, indicating the high purity of raw material understudy. X-ray diffraction of neat asphalt sample (AP-5 OSP 0 wt %) was analyzed and the diffractogram is presented in Figure 5. Figure 5 shows that most of the peaks appear at around 2θ value of 20° and 25°. The γ-peak, which occurs at approximately 2θ = 20°, mirrors the packing distance of saturated structure that comes from the X-rays scattered by the aliphatic chains or the condensed naphthenic rings. It has been reported that this band arises principally from paraffins order [47]. The (002) peak or graphene peak, which appears at about 2θ = 25°, is due to the diffraction of X-rays from the stacks of aromatic sheets. The (10) and (11) peaks, or (100) and (110) reflections, originate from the *in*-plane structure of the aromatic molecules. They refer to the first and second nearest neighbors in the ring compounds. Generally, the size of an aromatic sheet is often determined from the (10) peak (2θ = 40°), and not from (11) peak, due to its very weak intensity [48]. It is widely known that when the peaks in the XRD patterns are broader, the more short range exists in that structure type. This case comprises the unfilled and OSP-filled asphalts. On the other hand, when the XRD pattern peaks are sharper and narrower, the more highly crystalline phase with high

degree of long-range order exists. The oyster shell powder meets this criterion. As demonstrated by XRD patterns, with the increase in OSP dosage from 5 to 15 wt %, the intensity of the $CaCO_3$ peaks gradually increased without affecting the XRD profile of the base bitumen. This suggests that OSP exists stably in the binder structure, which means that its addition did not cause any change in the crystalline phase of bitumen (governed chiefly by asphaltene compound). Accordingly, it can be assumed that the OSP has no chemical reaction in the asphalt system and exists independently with only filling effect.
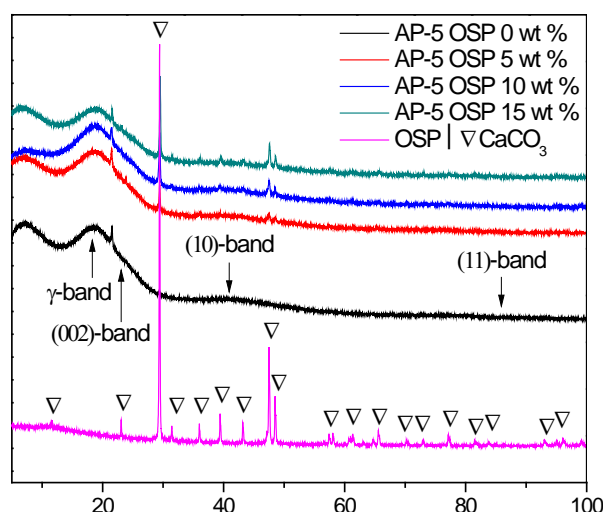

Figure 5. XRD patterns of OSP, neat asphalt, and OSP-filled asphalts.

3.5. Thin-Layer Chromatography-Flame Ionization Detection (TLC-FID)

To gain deeper insight into the impact of oyster shell powder (OSP) on the composition of asphalt cement, this latter was divided into SARA (i.e., saturates, aromatics, resins, and asphaltenes) fractions by using standard procedure based on adsorption chromatography (e.g., TLC-FID) [32]. Figure 6 pinpoints the distribution of SARA type hydrocarbons in the base asphalt (i.e., AP-5 OSP 0 wt %) and asphalt treated with different proportions (e.g., 5, 10, and 15 wt %) of OSP. Curiously, it shows that the composition of asphalt changed after the addition of OSP. The fraction of aromatics components decreased; meanwhile, the fraction of resins increased. The remaining species such as saturates and asphaltenes did not undergo any significant changes. The changing of such composition fraction implies that the aromatics in lighter fractions of asphalt were more probably changed to resins. In other terms, it seems that the aromatics were selectively interacted with OSP surface [49,50] and readily converted into resin-like structures (see Figure 7). The oyster shell powder (i.e., $CaCO_3$) with high calcium content is naturally hydrophilic material and tends to create strong bonds with hydrophobic organic compounds such as bitumen. The strong bonding between the calcite (mainly calcium sites) and adsorbate aromatic molecules most likely involved the carboxylic, hydroxylic, and amines groups; some van der Waals and electrostatic interactions may have also occurred [49,50]. This is a very interesting finding that necessitates further in-depth investigation.
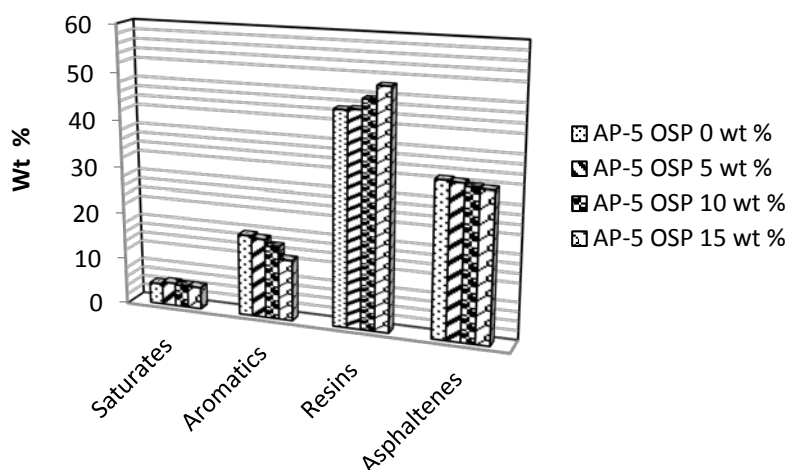
Figure 6. Chemical composition of unfilled and OSP-filled asphalts.
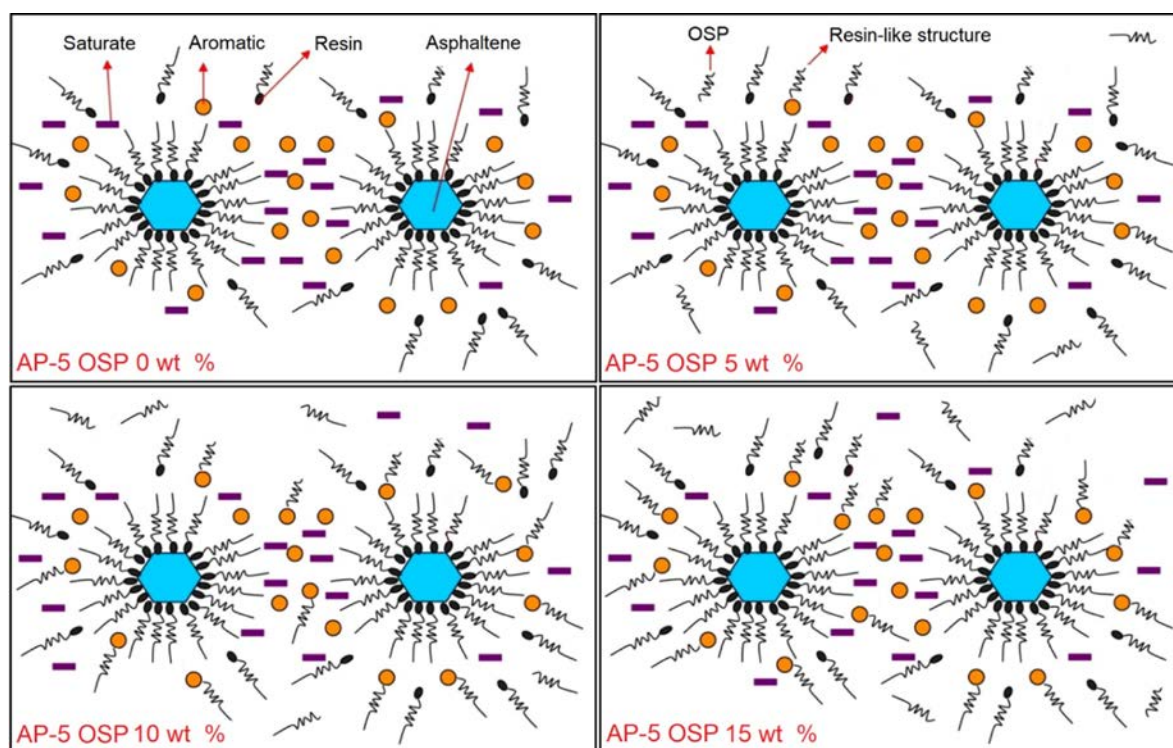
Figure 7. Adsorption of aromatic components on oyster shell powder surface at different doses (e.g., 0, 5, 10, 15 wt %) and creation of resin-like structures.

3.6. Conventional Asphalt Binder Tests (Penetration, Softening Point, and Ductility)

The results of empirical tests such as penetration, softening point, and ductility for unfilled and OSP-filled asphalts are given in Table 4. It is readily seen by reference to this Table that the physical properties of asphalt were greatly affected following the addition of OSP. The penetration and ductility of filled asphalt were decreased, whereas its softening point was increased.

The OSP essentially stiffens the binder due to three major reinforcement mechanisms:

1) Volumetric-filling reinforcement: the stiffening caused by the presence of rigid inclusions (e.g., mineral filler) in a less rigid matrix (e.g., viscoelastic binder).
2) Physicochemical reinforcement: the stiffening caused by the interfacial effects between filler particles and asphalt, including adsorption, absorption, and selective sorption.

Here, the treated asphalt efficiently creates a rigid layer, which leads to a higher net volume concentration of rigid matter, increasing thereby the mastic stiffness.

3) Particle-interaction reinforcement: the stiffening beyond physicochemical reinforcement and volume filling. This effect increases with increasing filler dosage, as rigid matter accumulates a skeletal framework form [51].

Too much OSP could over-stiffen the road surface, making it more susceptible to cracking or raveling. Therefore, special caution should be taken when using this biofiller. The increase in softening point is desired, as the binder with high softening point is less susceptible to permanent deformation. Therefore, asphaltic mixtures prepared with oyster shell powder (OSP) are initially expected to have better rutting performance. Also, the softening point variation is quietly similar to viscosity variation. Actually, these two physical properties are firmly linked, since it is logical to assume that asphalts with high softening point are also more viscous than those that have low softening point. The OSP does not form a homogenous liquid with asphalt, but remains a solid, which has an impact on the increase in viscosity, which is an indicator of fluid resistance against shear [52,53]. By increasing the addition of a solid that is insoluble in asphalt, one should expect the increase of mixture viscosity, regardless of the asphaltene content in the base asphalt.

This prediction was also made based on direct observation taken during the mixing process. Astonishingly, it was noticed that the blends were becoming overly viscous, with further OSP incorporation (particularly with 15 wt %). This increase in viscosity is attributed essentially to the higher asphaltene content of the base AP-5 asphalt (ca. 32.90 wt %). It has been reported that the asphalt with greater asphaltene content, when compounded with basic filler (e.g., $CaCO_3$), will result in higher viscosity, while acid filler (e.g., granite) will result in lower viscosity [54]. If a large quantity of biofiller is added, the HMA (i.e., hot-mix asphalt) blend will become difficult to dump, spread, and compact. Accordingly, special attention should be bestowed on the selected OSP dose in order to achieve an adequate consistency.

Table 4 also illustrates that, in all cases, as the mineral filler content increased in the asphalt cement, the ductility (at 25 °C) decreased very rapidly. These results revealed that the mastics tend to crack due to the asphalt elongation, which decreased as the OSP content increased. Low ductility indicates that the bitumen is brittle and will fracture before deforming much under a tensile load. Owing to its high surface area, the OSP formed strong bonds with the binder matrix, promoting the bitumen cohesion.

For a great numerous technical applications, the changes in consistency between 0 °C and the temperature of softening point form a highly important and much-discussed quality consideration in judging the utility of an asphaltic bitumen. This property of temperature susceptibility as reflected by penetration index (PI) proposed by Pfeiffer and van Doormaal has been related to various mastic properties and OSP contents. According to Table 4, the PI values of asphalt binder were increased as the OSP content increased in the mastic. Therefore, the temperature susceptibility of binders was decreased by increasing the quantity of OSP. The PI varies generally from −3 to +7 [1]. Asphalt with high thermal susceptibility has PI of −3 (e.g., most sol-asphalts and those extracted from cracking processes), and asphalt binder with PI of +7 (e.g., most gel-asphalts, blown asphalts) is insusceptible to variations in temperature [55]. Asphalt binder with higher PI yields less temperature susceptibility that leads to an improvement in rutting resistance and reduction in low temperature cracking [56]. In light of information available from conventional test methods, it can be reasonably assumed that the mixing of asphalt binder with OSP could have a positive impact on improving temperature susceptibility, rutting performance, and low temperature cracking.

Table 4. Physical properties of unfilled and OSP-filled asphalts.

Sample	Penetration at 25 °C (dmm)	Penetration Index (PI)	Softening Point (°C)	Ductility at 25 °C (cm)
AP-5 OSP 0 wt %	60.00	−0.77	50.00	110.50
AP-5 OSP 5 wt %	58.20	−0.11	53.00	103.33
AP-5 OSP 10 wt %	55.10	+0.80	57.70	95.10
AP-5 OSP 15 wt %	52.50	+1.24	60.50	89.50

3.7. Dynamic Shear Rheometer (DSR) Test

3.7.1. Rutting Performance (G*/sin δ)

The high temperature performance grade of each bitumen sample was determined using DSR (i.e., dynamic shear rheometer) test results (G*/sin δ) and the Superpave (i.e., Superior Performance Asphalt Pavement) binder specification. Based on the specification to minimize rutting, G*/sin δ at 10 rad s^{-1} must have a minimum of 1 kPa for unaged bitumen sample and 2.2 kPa for rolling thin-film oven (RTFO)-aged bitumen sample [38]. The Superpave rutting parameter G*/sin δ is inversely proportional to the dissipated energy, and thus higher G*/sin δ will have lesser dissipated energy, and thus higher rut resistant. Figure 8 shows the DSR results, at various temperatures (e.g., 52, 58, 64, and 70 °C), for the unaged base asphalt (i.e., AP-5 OSP 0 wt %) and unaged asphalt containing different fractions of OSP (e.g., 5, 10, 15 wt %). The performance grade of neat asphalt (i.e., AP-5 OSP 0 wt %) was 64 °C prior to failure at 70 °C. Whereas, the 5 and 10 wt % OSP-filled asphalt samples can resist rutting until 70 °C. Their rutting parameters (G*/sin δ) were higher than those of the neat asphalt sample. The G*/sin δ values recorded at 70 °C for 5, 10, and 15 wt % OSP, were 1175, 1484, and 832 Pa, respectively. The most outstanding value of rutting resistance was observed with 10 wt % OSP. High rutting parameter was observed from 52 °C to 70 °C. The rutting resistance increased as the OSP content increased up to 10 wt % OSP, followed by a decrease with 15 wt % OSP. This may be due to the agglomeration among the OSP particles with further increment of additive in asphalt cement blends. Generally, this finding showed that the OSP increased the stiffness of the virgin bitumen. The mineral particles (i.e., CaCO$_3$) seemingly reinforced the bitumen matrix by increasing the bond strength between the filler and binder combinations, improving thereby the cohesion of the bitumen. Consequently, the bitumen properties were enhanced by increasing the stiffness and improving rutting performance.

The RTFO-asphaltic samples shown in Figure 9 demonstrate clearly that both the unfilled and 15 wt % OSP-filled asphalt samples resisted rutting until 64 °C before failing at 70 °C. After short-term aging, all the samples obviously became markedly stiff, thereby increasing the rutting resistance. The asphalt mixtures containing 5 and 10 wt % OSP showed higher performance compared to the neat asphalt and asphalt treated with 15 wt % OSP at all the tested temperatures practically. These results are in tune with those obtained from unaged OSP-asphalt mastic samples. The rutting resistance values of the asphalt filled with 10 wt % OSP at 52 °C were 17250 Pa and 2794 Pa at 70 °C, which were the highest of all aged asphalt samples. Furthermore, rutting performance showed significant differences between the OSP contents. The 15 wt % OSP obtained the lowest rutting parameters at 64 °C and 70 °C with G*/sin δ of 2960 and 1886 Pa, respectively. This asphalt exhibited a lower stiffness than the OSP-filled asphalt samples during short-term aging. The large surface area of the OSP absorbs and distributes the heat rapidly relative to the unfilled asphalt, which stands alone at distributing the heat in the slow rate and causing the bitumen to age swiftly. Therefore, 10 wt % OSP was the optimum dose that could retard the aging of the bitumen at higher temperature compared with other OSP fractions (e.g., 5 and 15 wt %). The results of penetration and softening point tests shown in Table 4 confirm the positive impact of OSP on high temperature of filled bitumens.
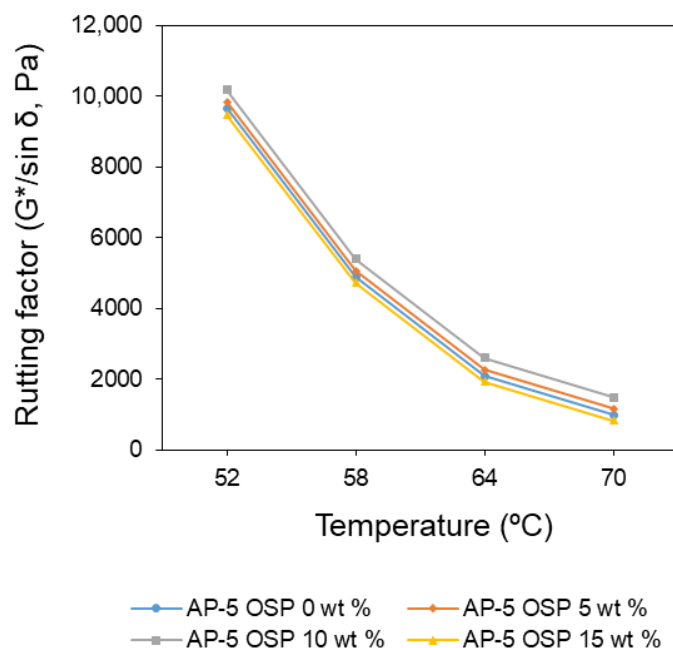
Figure 8. Effect of temperature on the rutting parameter of unfilled and OSP-filled asphalts under unaged condition.
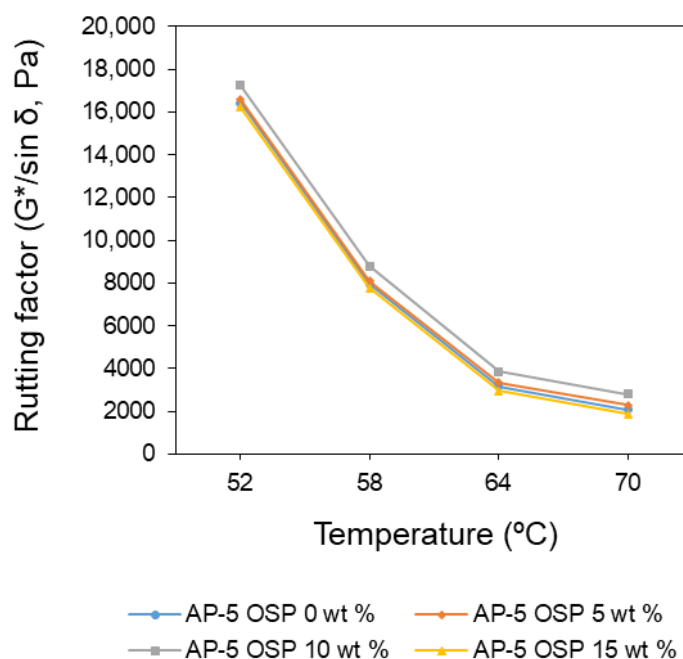
Figure 9. Effect of temperature on the rutting parameter of unfilled and OSP-filled asphalts under short-term aging condition (RTFO: rolling thin-film oven).

3.7.2. Fatigue Cracking Performance (G*.sin δ)

G*.sin δ is the fatigue cracking factor in the Superpave (i.e., Superior Performance Asphalt Pavement) binder Specification. Requirement to address fatigue cracking in Superpave binder specification is that G*.sin δ at 10 rad s^{-1} shall not exceed 5000 kPa [38]. Thus, low values of G* and δ are considered desirable attributes from the standpoint of resistance to fatigue cracking. The higher G*.sin δ value, the more fatigue cracking is susceptible the bitumen. Figure 10 displays the fatigue cracking performance of the base asphalt (i.e., AP5 OSP 0 wt %) and asphalts treated with different

concentrations of OSP (e.g., 5, 10, and 15 wt %) under the PAV (i.e., pressure aging vessel) condition. The increasing trend of the master curve highlighted that the treated samples resist fatigue cracking from intermediate to lower temperatures (e.g., 31, 28, 25, 22, and 19 °C). The failure temperature was reached when the fatigue cracking parameter (G*.sin δ) exceeded 5000 kPa. From the foregoing data it is obvious that 15 wt % OSP exhibited G*.sin δ value of 5325 kPa, which failed at temperature of 19 °C. Also, the failure temperature of the base asphalt sample was attained at 19 °C, with G*.sin δ value of 5225 kPa. Similarly, failure temperature was observed on 5 wt % OSP-filled asphalt with a recorded G*.sin δ value of 5125 kPa. The optimum was reached only with 10 wt % OSP-filled asphalt sample, because it showed lower G*.sin δ value than the base asphalt and met the Superpave minimum requirement at 19 °C (G*.sin δ = 4925 kPa). It becomes clear that 10 wt % OSP exhibits higher resistance to fatigue cracking as compared with other OSP contents.

The higher geometric irregularity of the OSP yields higher adsorption intensity. This effect will result in a strengthening of the filler-binder bonds and a relative increase in the fixed binder amount, while the mastic will get higher consistency and strength (i.e., stiffness) than the control specimen. However, during the service life of the road pavement, bitumen tends to stiffen due to oxidation phenomenon, leading to fatigue cracking. In this investigation, the absorbed heat in the OSP-filled asphalts during high temperatures was stored longer than that in the neat asphalt. Thus, during the decrement of test temperature, the OSP slowly released the heat and the heat loss under equilibrium condition, which helped to maintain the viscoelasticity of the bitumen instead of rapidly releasing the heat and stiffening its matrix. Overall, an intermediate dose of OSP (i.e., 10 wt %) can retard the aging process effectively as compared with 5 and 15 wt % OSP-asphalt mastic samples. The large surface area of the OSP particles delayed the heat loss, especially, when more appropriate amounts were added. With the viscoelasticity of the bitumen and its capacity to resist rutting and cracking under consideration, 10 wt % OSP was considered as the optimum filler dose for bitumen because of its superior performance compared to that of the control binder.
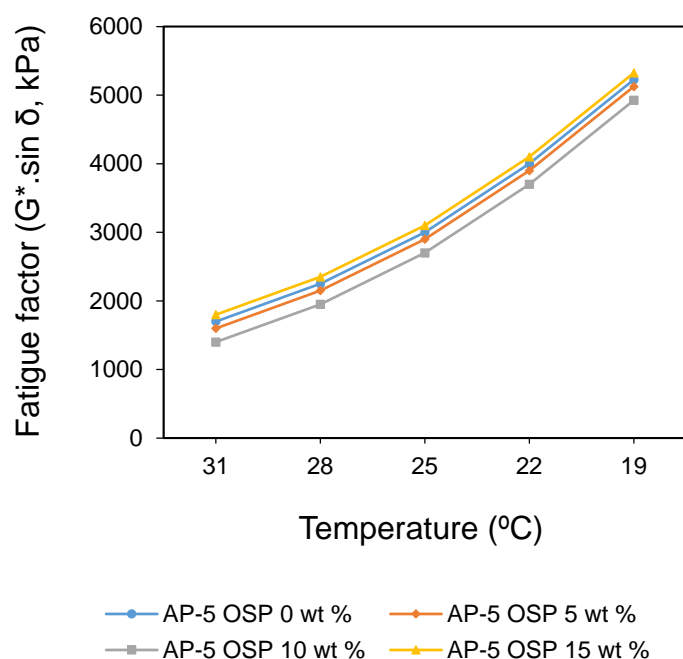
Figure 10. Effect of temperature on the fatigue cracking parameter of unfilled and OSP-filled asphalts under long-term aging condition (PAV: pressure aging vessel).

3.8. Scanning Electron Microscope (SEM)

The possible interaction between OSP particles and asphalt binder was further assessed by SEM imaging analysis for a better understanding of the rheological findings. This approach permitted the identification of inorganic filler distribution inside the bituminous matrix, thus helping to explain the

differences detected in fatigue and rutting behaviors between unfilled and OSP-filled asphalts. Figures 11 and 12(A1,2–D1,2) display the SEM patterns of OSP, base asphalt (i.e., AP-5 OSP 0 wt %), and asphalt treated with different concentrations of OSP (e.g., 5, 10, 15 wt %). The SEM micrographs were taken at different levels of magnification (e.g., ×100, ×500, and ×3000). In the low magnification SEM images (Figure 11, ×100), it can clearly be seen that the OSP comprises some large particles and high fraction of fine particles, which resulted in a more heterogeneous distribution. The comminuted powder exhibits an irregular crystal structure of densely attached fine grains (e.g., width 1–130 μm, length 1–246 μm) caused probably by the mechanical effect during dry grinding. These results are also being well observed in particle size distribution curves in Figure 3. The filler is detectable as angular and rough particles with schistous structure and low propensity to agglomerate.

By examining the SEM images of AP-5 asphalt treated with 5 and 10 wt % OSP, the presence of filler in the asphaltic matrix can be easily detected in the form of uneven distributed aggregates. On the contrary, it is worth mentioning that in the case of neat asphalt (i.e., AP-5 OSP 0 wt %), the SEM image reveals the existence of a continuous network that is characterized by a uniform, smooth, and homogeneous surface. As seen in Figure 12 (B1,2,C1,2), the OSP in different shapes (i.e., mainly in flat shapes) could be obviously identified in the asphalt bulk. Generally, it can be found that the oyster shell powder (i.e., dispersed phase) and asphaltic material (i.e., viscoelastic matrix) exist independently, establishing that there is perhaps no chemical reaction between them. Hence, as one mineral admixture, OSP mainly plays its role through "micro-aggregate filling effect" and "morphological effect" in the bituminous material. The micro-aggregate filling effect means that the micro-particles of mineral admixture spread evenly across the basic phase of asphalt with the consolidation and filling effects. On the other side, the morphological effect arises from the effect caused by grain composition, surface property, internal structure, external morphology, and other physical features of the particles. These two effects supplement each other and are interrelated.

The oyster shell powder obtained with dry ball grinding is finer and barely homogeneous, and thus its addition made the particle stacking in the asphalt much closer. It can be assumed that there is fairly better interface binding among particles, so the asphalt strength is improved, especially for early strength (generated particularly with 5 and 10 wt % of filler). Therefore, when the content of added OSP is increased to 15 wt %, the asphalt strength (i.e., stiffness and hardness) shows an increased trend. This tendency to rise is largely dictated by the physical properties of oyster shell powder such as gradation, specific surface area, shape, and porosity. Oyster shell powder is an amorphous material that agglomerates at higher concentration and can significantly affect the mechanical properties of resultant composite.

Figure 11. Scanning electron microscope (SEM) micrographs of oyster shell powder (OSP) obtained with dry ball grinding at different magnifications ×100 (**A**) and × 500 (**B**).

The SEM micrographs of 5 and 10 wt % OSP-filled asphalts (Figure 12(B1,2,C1,2)) display a more uniform material, since filler particles are well embedded in the bituminous phase, creating a more

efficiently collaborative morphological structure between bitumen and filler. Nevertheless, in the case of the 15 wt % OSP-filled asphalt (Figure 12(D1,2)), it can be seen that there are certain number of holes or large amount of voids (highlighted with orange and red circles) due to detachment of OSP grains. This is most likely due to the poor bonded interfacial area between filler and binder matrix, which causes brittle deformation of the bio-composite. In turn, this implies the formation of agglomerate structures (i.e., irregular particle clusters or flocs) in the bituminous phase, thereby creating an internal discontinuous network that is unable to properly englobe the filler particles. Contrarily, with regard to the 5 and 10 wt % OSP-filled binders, the bitumen is able to entirely coat the filler particles. This finding further supports the results obtained in terms of rutting and fatigue performances of the 15 wt % OSP-treated asphalts as compared to those of the 5 and 10 wt % OSP-treated ones.
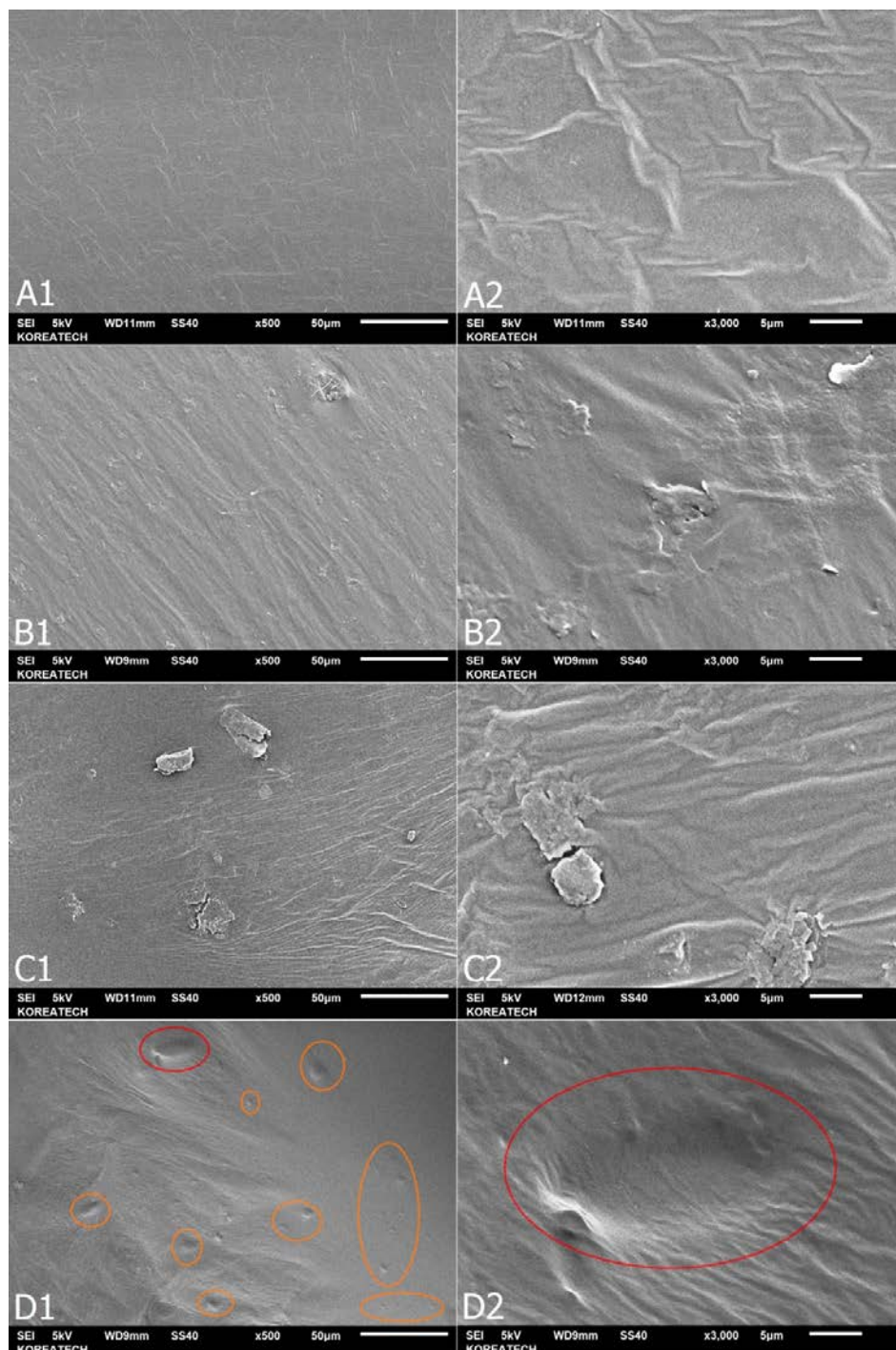
Figure 12. Scanning electron microscope (SEM) micrographs of unfilled and OSP-filled asphalts taken at ×500 [denoted with number 1] and ×3000 [denoted with number 2] magnifications. (**A**) AP-5 OSP 0 wt %; (**B**) AP-5 OSP 5 wt %; (**C**) AP-5 OSP 10 wt %; (**D**) AP-5 OSP 15 wt %.

3.9. Thermogravimetric Analysis (TGA/DTGA)

Response of the bio-composite specimens to thermal loads was assessed using TGA/DTGA (i.e., thermogravimetric and derivative thermogravimetric). The percentage of weight loss (i.e., degradation, wt %) versus temperature increase is displayed in Figure 13. TGA analysis was performed under an inert atmosphere of nitrogen (i.e., N_2) and from 25 °C to 1000 °C. This temperature range was chosen, not only to simulate the temperature at which the HMA (i.e., hot mix asphalt) is produced (150–190 °C) but also to gain some insight into the material stability when it is subjected to higher temperatures. The TGA/DTGA curves of OSP, and unfilled and OSP-filled asphalts, are depicted in Figures 13 and 14, respectively. Table 5 lists the different events that occurred during the experiment. As shown in Figure 13, it is apparent that there are three typical decomposition stages for neat asphalt (i.e., AP-5 OSP 0 wt %): (1) The first phase of mass loss happened in the temperature up to around 362.23 °C, corresponding to release of oil content from the asphaltic samples (i.e., mainly saturates and aromatics). (2) Afterwards, there was a minor variation in weight, and then substantial weight loss occurred again in the second stage from approximately 362.23 °C to 457.56 °C, which was primarily caused by the thermal degradation of hydrocarbonaceous materials (i.e., resins and some portion of asphaltene fraction). (3) The last stage occurred, corresponding to the combustion of the remaining asphaltenes and the formation of char residues (ca. 14.29 wt %) [57].

TGA was conducted also to determine the calcination characteristics of the oyster shell powder. The TGA profile of OSP is shown in Figure 13. It is evident that in the first stage, the humidity was removed from OSP (i.e., $CaCO_3$), i.e., only 1.33 wt %. According to European Standards UNE-EN 13043 [58], the moisture content of filler for bituminous mixtures should be below 1 wt %. However, OSP was found to contain 1.33 wt % of humidity, which may cause stripping in HMA (i.e., hot mix asphalt) pavements and ultimately result in premature failure. Accordingly, the water should be removed to ensure proper adhesion between bitumen and the aggregate surface, thus providing the mixture with adequate resistance to moisture, the most deleterious factor affecting road pavement quality [59]. On the other hand, like many other additives (e.g., natural and synthetic zeolites) [60–62], the water-containing OSP could be used in the production of WMA (i.e., warm mix asphalt). The most common WMA technology utilizes asphalt foaming by adding a small amount of water into the hot binder or directly to the aggregate and asphalt mixer [60]. This process allows the asphalt mixture to have good workability during laying and compaction, and durability during traffic exposure [63].

At the second stage from 641.31 °C to 710.76 °C, the total weight loss referred to loss of carbon dioxide (CO_2) as 42.78 wt %. Theoretical weight loss is known to be 44 wt %. In the third stage at 710.76–999.98 °C, the total weight loss was 45.09 wt %. There was a considerable change in the weight of the oyster shell powder as the temperature was raised from 25.21 °C to 999.98 °C due to calcination reactions, which commenced at 641.31 °C; however, the complete calcination of OSP resulting in a phase-change of the sample was only achieved at 999.98 °C. A major component of the oyster shell powder was identified as pure $CaCO_3$ at the temperature of 641.31 °C. The moisture and organic content removal was achieved below 641.31 °C. When temperature was raised from 641.31 °C to 710.76 °C, $CaCO_3$ (i.e., calcite, calcium carbonate) and CaO (i.e., lime, calcium oxide) were identified as the main components of the OSP. The calcination under inert atmosphere led to a mass loss of 45.09 wt %. A major component of the oyster shell powder at temperatures above 710.76 °C was identified as pure crystalline CaO. It can be admitted that most of the oyster shell was transformed to CaO by final pyrolysis at temperatures higher than 710.76 °C. Hence, this infers that the optimum temperature of calcination of oyster shell was reached at a temperature range of around 641.31 °C.

The initial degradation temperatures (T_{onset}) of unfilled and OSP-filled asphalts were determined by the bi-tangent method and presented in Table 5. Owing to the addition of 5 and 10 wt % OSP, the thermal stability of the mastics was well developed, but not with 15 wt %. The oyster shell powder is

a sort of inorganic material, which is difficult to degrade like organic material. When it interacts with the asphalt matrix, it can obviously improve the thermal stability of resultant composite. This is similar to the physical properties mentioned previously, and OSP not only strengthens the physical properties (i.e., stiffness) but also increases the thermal stability.
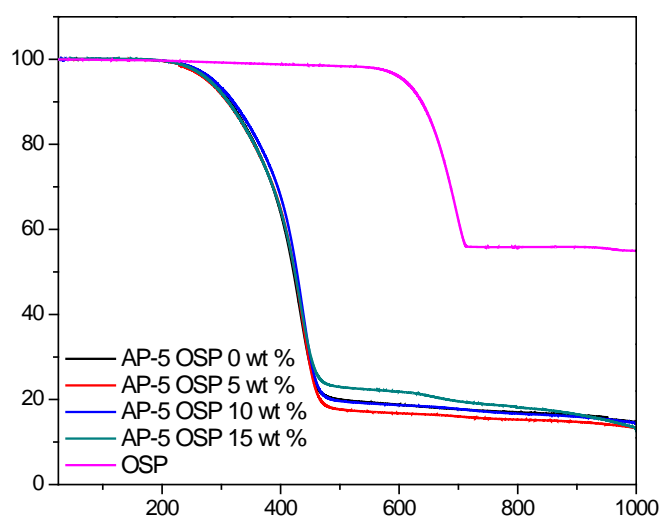

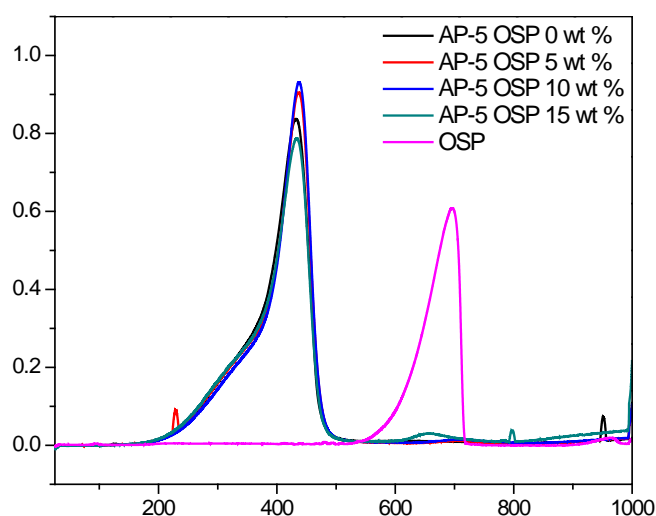**Figure 13.** TGA thermograms of OSP, neat asphalt, and OSP-filled asphalts.

Figure 14. DTGA thermograms of OSP, neat asphalt, and OSP-filled asphalts.

Table 5. TGA and DTGA thermogram data of OSP, neat asphalt, and OSP/asphalt blends containing 5, 10, and 15 wt % OSP loading at heating rate of 10 °C min^{-1}.

Sample	TGA/DTGA (°C)						$-\Delta W$ (wt %)
	Stage 1	**Stage 2**	**Stage 3**	T_{onset}	T_{offset}	T_{max}	
OSP	25.21–641.31	641.31–710.76	710.76–999.98	641.31	710.76	695.89	54.91
AP-5 OSP 0 wt %	25.39–362.23	362.23–457.56	457.56–999.97	362.23	457.56	432.27	14.29
AP-5 OSP 5 wt %	25.25–369.64	369.64–460.60	460.60–999.98	369.64	460.60	437.14	13.01
AP-5 OSP 10 wt %	25.14–374.47	347.47–460.72	460.72–999.98	374.47	460.72	437.80	14.11
AP-5 OSP 15 wt %	25.15–362.42	362.42–458.33	458.33–999.98	362.42	458.33	433.65	12.56

T_{onset}: onset of thermal degradation (°C). T_{offset}: offset of temperature of final loss (°C). T_{max}: maximum decomposition temperature (°C). ΔW: carbonaceous residue at 1000 °C (wt %).

3.10. Differential Scanning Calorimetry (DSC)

The differential scanning calorimetry (DSC) was carried out to elucidate the impact oyster shell powder (OSP) on the thermal transitions of asphalt cement. The effect of OSP content (e.g., 0, 5, 10, and 15 wt %) on the glass transition temperature (T_g) of binders obtained from Figure 15 is illustrated in Table 6. Figure 15 demonstrates several thermal effects of the base asphalt (i.e., AP-5 OSP 0 wt %): (a) At very low temperatures (from −34 °C to −15 °C), the increase in heat capacity can be attributed to the first glass transition temperature (T_{g1}) within the hydrocarbon matrix. It arises mainly from the maltene phase (i.e., a mixture of saturates, aromatics, and resins components) and is the most prominent transition. (b) Above T_{g1}, a second glass transition temperature (T_{g2}) occurs. It comes from a maltene-asphaltene interfacial zone, which is most likely rich in resins. For convenience's sake, it can be defined as "an interphase", even though it may not be a strictly separate phase [64,65]. It becomes clear that the pure AP-5 asphalt is a mixture, and this mixture is not completely homogenous, since it shows more than one T_g. Surprisingly, no obvious endothermic or exothermic effects have been shown in the DSC thermograms. This may be because the AP-5 asphalt contains inconsiderable amount of saturates (ca. 4.47 wt %; *n*-alkanes (waxes/paraffins), *iso*-alkanes, and cyclo-alkanes), which will bring a possible positive impact on crack susceptibility due to the absence of wax. The DSC curve for OSP, given in Figure 16, exhibits only a sharp endothermic peak located at 820.50 °C that can be ascribed to the decomposition of $CaCO_3$ and possible removal of absorbed water molecules that occur according to the following dissociation equation: $CaCO_3$ (s) + Heat → CaO (s) + CO_2 (g) (1). This reaction is also confirmed by TGA/DTGA analysis.

In inert atmosphere, some differences stand out. Figure 16 indicates that there is change in glass transition temperature (T_g) between unfilled and OSP-filled asphalt samples. This fact implies that the presence of OSP affected the T_g of asphalt to some extent. The DSC data of neat asphalt and OSP-asphalt mastics filled with various contents of OSP (e.g., 5, 10, and 15 wt %) are outlined in Table 6. The first glass transition peak temperature (T_{g1}) of OSP/asphalt composites was smaller than that of neat asphalt. As the filler content increased to 10 and 15 wt %, the T_{g1} dropped from −26.70 (for neat asphalt: AP-5 OSP 0 wt %) to −28.91 °C and to −28.12 °C, respectively. However, the OSP/asphalt composite was also found to have a slightly higher glass transition peak temperature than the base asphalt. The temperature slightly rose from −26.70 °C to −25.61 °C with a filler dose of 5 wt %. The T_g, though, changed irregularly with the OSP content.

This probably happened because when incorporating filler into a viscoelastic matrix, the binder will adsorb on the filler surface, creating a monomolecular layer, which causes an increase in T_g, but with higher concentration; the filler will form a superstructure (i.e., chains), which changes the whole inner structure of the binder system, thereby lowering T_g. Also, this could be related to the physicochemical interaction effect, which originates from the adsorption of polar groups in asphalt (mainly resins and asphaltenes) onto the surface of OSP particles. This adsorption is partially responsible for the observed changes in thermal properties (e.g., glass transition temperature, T_g) and the rheological properties (e.g., stiffness and viscosity) of OSP/asphalt blends. The amount of polar groups adsorbed is seemingly found to be dependent on the Braunauer-Emmett-Teller (BET) surface area of the filler but not on the chemical composition of the filler or bitumen [66]. The higher the BTE surface area (e.g., 10 and 15 wt % OSP), the greater the amount of polar groups adsorbed and the lower the glass transition temperature, and vise-versa (with 5 wt % OSP) [66]. The reduction in the glass transition temperature indicates that this adsorption phenomenon results in asphalt softening. The data deducted from DSC studies indicates that higher content of OSP will worsen the low-temperature performance of bitumen; however, lower content (≤5 wt %) will improve it [67,68]. Further BBR (i.e., bending beam rheometer) and DMA (i.e., dynamic mechanical analysis) studies are absolutely necessary to prove this assumption.
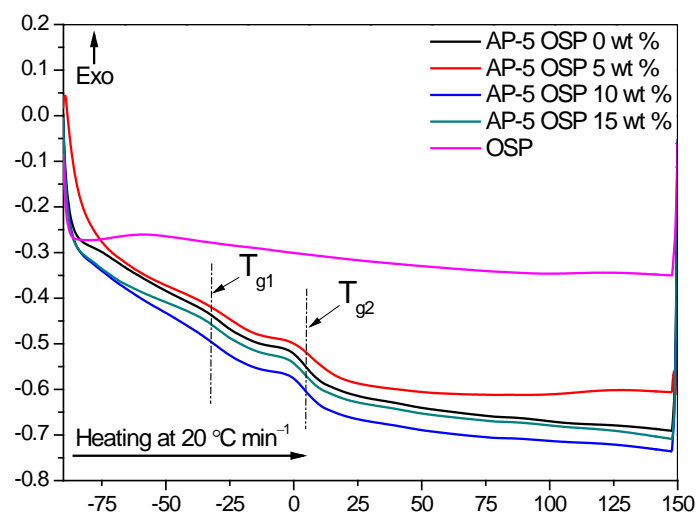
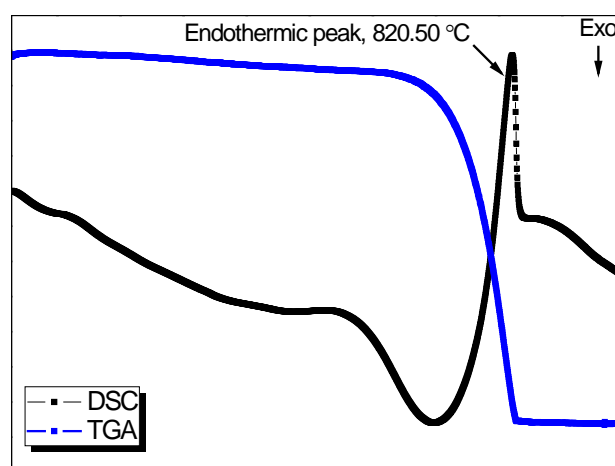**Figure 15.** DSC thermograms of OSP, neat asphalt, and OSP-filled asphalts.

Figure 16. STA (TGA/DSC) measurement of OSP (sample mass 11.151 mg) in Alumina crucibles at a heating rate of 10 K min^{-1} in argon atmosphere (50 mL min^{-1}).

Table 6. DSC thermogram data of OSP, neat asphalt, and OSP/asphalt blends containing 5, 10, and 15 wt % OSP loading at heating rate of 20 °C min^{-1}.

Sample	Thermal Parameter			
	T_{g1} (°C)	ΔCp_1 (J g·°C^{-1})	T_{g2} (°C)	ΔCp_2 (J g·°C^{-1})
OSP	†	†	†	†
AP-5 OSP 0 wt %	−26.70	0.1946	5.17	0.2360
AP-5 OSP 5 wt %	−25.61	0.2083	9.37	0.2554
AP-5 OSP 10 wt %	−28.91	0.2343	6.08	0.2559
AP-5 OSP 15 wt %	−28.12	0.2077	5.74	0.2469

T_{g1}: glass transition of maltenic phase (°C). T_{g2}: glass transition of maltenic–asphaltene interphase region (°C). †: absence of glass transition temperature in DSC thermogram of OSP.

4. Conclusions

To recover the oyster shell waste (OSW) for potential use, engineers, researchers, generators, and regulators need to be aware of the properties of these materials, how they can be used, and what limitations may be associated with their use. This preliminary study was conducted mainly to develop a means of converting WOS into useful filler in road pavement construction. The effect of different concentrations (e.g., 0, 5, 10, 15 wt %) of oyster shell powder (OSP) on the bitumen performance was examined. FT-IR and XRD data demonstrated that no apparent reactions have occurred between the inorganic filler and the asphalt cement. In response to filler treatment, TLC-FID revealed that the resin content increased at the expense of aromatic content. Due to the good distribution of OSP particles in the bituminous matrix, the thermal stability of bio-composites was achieved only with 5 and 10 wt %, as compared to plain bitumen. On the other hand, SEM analysis disclosed that a higher concentration (i.e., 15 wt %) of filler provoked an agglomeration and affected the bitumen morphology and microstructure. DSC results indicated that a lower content of natural $CaCO_3$ reduced the glass transition temperature (T_{g1}) of binder; however, intermediate and higher contents increased it. The increase in hardness and stiffness, following the addition of mineral filler, was reflected by a decrease in penetration and ductility, and an increase in softening point of blends. The incorporation of OSP also enhanced the fatigue and rutting resistance of filler-asphalt mastics in comparison to control sample. The results of incremental increases in filler content up to 10 wt % were shown to be beneficial in all respects. In short, it can be concluded that OSP could be used as alternative filler in hot-mix asphalt (HMA). However, further comparative investigations with conventional mineral filler are required before integrating effectively this biofiller into practice. Future work may involve the inclusion of additional rheological techniques such as bending beam rheometer (BBR) test, rotational viscometer test, direct tension tester (DTT), etc.

Author Contributions: Nader Nciri performed the research, analyzed, and interpreted the data, and wrote the paper. Taesub Shin and Haksoo Lee conceived and designed the experiments. Namjun Cho supervised the project.

References

1.　Read, J.; Whiteoak, D. *The Shell Bitumen Handbook*, 5th ed.; Thomas Telford Publishing: London, UK, 2003; p. 464, ISBN-13:978-0727732200.
2.　Transportation Research Board of the National Academies. Chapter 4. Aggregates. In *NCHRP (National Cooperative Highway Research Program) REPORT 673—A Manual for Design of Hot Mix Asphalt with Commentary*; National Academy of Sciences: Washington, DC, USA, 2011; pp. 28–45, ISBN 978-0-309-15564-9.
3.　Lee, D.Y. The Effect of Filler on Asphalt Cement Mastics. Ph.D. Thesis, Iowa State University of Science and Technology, Ames Iowa, USA, 1964.
4.　Chen, J.S. Rheological Properties of Asphalt-Mineral Filler Mastics. *J. Jpn. Soc. Civil Eng.* **1997**, *36*, 269–277.
5.　Kim, M.; Buttlar, W. Stiffening Mechanisms of Asphalt-Aggregate Mixtures. *Transp. Res. Rec. J. Transp. Res. Board* **2010**, *2181*, 98–108.
6.　Underwood, B.S.; Kim, Y.R. Experimental investigation into the multiscale behavior of asphalt concrete. *Int. J. Pavement Eng.* **2011**, *12*, 357–370.
7.　Clopotel, C.; Velasquez, R.; Bahia, H. Measuring physico-chemical interaction in mastics using glass transition. *Road Mater. Pavement* **2012**, *13*, 304–320.
8.　Rigden, P.J. The use of fillers in bituminous road surfacings. A study of filler-binder systems in relation to filler characteristics. *J. Chem. Technol. Biot.* **1947**, *66*, 299–309.
9.　Heukelom, W. The role of filler in bituminous mixes. *J. Assoc. Asph. Paving Technol.* **1965**, *34*, 396–429.

10. Anderson, D.A. Mechanical Behavior and Reinforcement of Mineral Filler-Asphalt Mixtures. *J. Assoc. Asph. Paving Technol.* **1973**, *42*, 37–66.

11. Craus, J.; Ishai, I.; Sides, A. Some physico-chemical aspects of the effect and the role of the filler in bituminous paving mixtures. *J. Assoc. Asph. Paving Technol.* **1978**, *46*, 558–588.

12. Davis, C.; Castorena, C. Implications of physico-chemical interactions in asphalt mastics on asphalt microstructure. *Constr. Build. Mater.* **2015**, *94*, 83–89.

13. Fini, E.H.; Al-Qadi, I.L.; You, Z.; Zada, B.; Mills-Beale, J. Partial replacement of asphalt binder with bio-binder: Characterization and modification. *Int. J. Pavement Eng.* **2012**, *13*, 515–522.

14. Dhasmana, H.; Ozer, H.; Al-Qadi, I.L.; Zhang, Y.; Schideman, L.; Sharma, B.K.; Chen, W.T.; Minarick, M.J.; Zhang, P. Rheological and Chemical Characterization of Biobinders from Different Biomass Resources. *Transp. Res. Rec. J. Transp. Res. Board* **2015**, *2505*, 121–129.

15. Guarin, A.; Khan, A.; Butt, A.A.; Birgisson, B.; Kringos, N. An extensive laboratory investigation of the use of bio-oil modified bitumen in road construction. *Constr. Build. Mater.* **2016**, *106*, 133–139.

16. Kowalski, K.J.; Król, J.B.; Bańkowski, W.; Radziszewski, P.; Sarnowski, M. Thermal and Fatigue Evaluation of Asphalt Mixtures Containing RAP Treated with a Bio-Agent. *Appl. Sci-Basel* **2017**, *7*, 216, doi:10.3390/app7030216.

17. Król, J.B.; Niczke, Ł.; Kowalski, K.J. Towards Understanding the Polymerization Process in Bitumen Bio-Fluxes. *Materials* **2017**, *10*, 1058, doi:10.3390/ma10091058.

18. Chen, M.; Lin, J.; Wu, S. Potential of recycled fine aggregates powder as filler in asphalt mixture. *Constr. Build. Mater.* **2011**, *25*, 3909–3914.

19. Chandra, S.; Kumar, P.; Feyissa, B.A. Use of Marble Dust in Road Construction. *Road Mater. Pavement* **2002**, *3*, 317–330

20. Modarres, A.; Rahmanzadeh, M. Application of coal waste powder as filler in hot mix asphalt. *Constr. Build. Mater.* **2014**, *66*, 476–483.

21. Saltan, M.; Öksüz, B.; Uz, V.E. Use of glass waste as mineral filler in hot mix asphalt. *Sci. Eng. Compos. Mater.* **2015**, *22*, 271–277.

22. Sargin, Ş.; Saltan, M.; Morova, N.; Serin, S.; Terzi, S. Evaluation of rice hush ash as filler in hot mix asphalt concrete. *Constr. Build. Mater.* **2013**, *48*, 390–397.

23. Jeffry, S.N.; Jaya, R.P.; Hassan, N.A.; Yaacob, H.; Mirza, J.; Drahman, S.H. Effect of nanocharcoal coconut-shell ash on the physical and rheological properties of bitumen. *Constr. Build. Mater.* **2018**, *158*, 1–10.

24. Kiruthiha, K.; Loshini, G.; Thivya, M. Strengthening of Flexible Pavement using Egg Shell as a Filler. *Int. J. Eng. Trends Technol. (IJETT)* **2015**, *21*, 483–486.

25. Arabani, M.; Babamohammadi, S.; Azarhoosh, A.R. Experimental investigation of seashells used as filler in hot mix asphalt. *Int. J. Pavement Eng.* **2014**, *16*, 502–509.

26. KDI (Korea Development Institute). *Report of Economic Policy (in Korean)*; KDI (Korea Development Institute): Seoul, Korea, 2002.

27. Yoon, G.L.; Kim, B.T.; Kim, B.O.; Han, S.H. Chemical–mechanical characteristics of crushed oyster-shell. *Waste Manag.* **2003**, *23*, 825–834.

28. Lee, J.Y.; Lee, C.H.; Ha, B.H.; Kim, S.C.; Lee, D.K.; Kim, P.J. Effect of Oyster Shell Meal on Improving Soil Microbiological Activity. *Korean J. Soil Sci. Fertil.* **2005**, *38*, 281–286.

29. Yang, E.I.; Yi, S.T.; Leem, Y.M. Effect of oyster shell substituted for fine aggregate on concrete characteristics: Part I. Fundamental properties. *Cement Concr. Res.* **2005**, *35*, 2175–2182.

30. Lee, C.H.; Lee, J.Y.; Ha, B.H.; Kim, P.J. Increased Available Phosphate by Shell Meal Fertilizer Application in Upland Soil. *Korean J. Soil Sci. Fertil.* **2005**, *38*, 52–57.

31. American Association of State Highway and Transportation Officials. *AASHTO T-37, Sieve Analysis of Mineral Filler for Hot Mix Asphalt (HMA)*; American Association of State Highway and Transportation Officials: Washington, DC, USA, 2011.

32. Masson, J.F.; Price, T.; Collins, P. Dynamics of Bitumen Fractions by Thin-Layer Chromatography/Flame Ionization Detection. *Energy Fuels* **2001**, *15*, 955–960.

33. American Society of Testing Materials (ASTM) International. *ASTM D36/D36M-14e1, Standard Test Method for Softening Point of Bitumen (Ring-and-Ball Apparatus)*; American Society of Testing Materials (ASTM) International: West Conshohocken, PA, USA, 2014.

34. American Society of Testing Materials (ASTM) International. *ASTM D113-07, Standard Test Method for Ductility of Bituminous Materials*; American Society of Testing Materials (ASTM) International: West Conshohocken, PA, USA, 2007.

35. American Society of Testing Materials (ASTM) International. *ASTM D5/D5M-13, Standard Test Method for Penetration of Bituminous Materials*; American Society of Testing Materials (ASTM) International: West Conshohocken, PA, USA, 2013.

36. Zhang, J.; Wang, J.; Wu, Y.; Wang, Y.; Wang, Y. Evaluation of the improved properties of SBR/weathered coal modified bitumen containing carbon back. *Constr. Build. Mater.* **2009**, *23*, 2678–2687.

37. Karmakar, S.; Roy, T.K. Effect of Waste Plastic and Waste Tires Ash on Mechanical Behavior of Bitumen. *J. Mater. Civil Eng.* **2016**, *28*, doi:10.1061/(ASCE)MT.1943-5533.0001484.

38. American Society of Testing Materials (ASTM) International. *ASTM D7175-15, Standard Test Method for Determining the Rheological Properties of Asphalt Binder Using a Dynamic Shear Rheometer*; American Society of Testing Materials (ASTM) International: West Conshohocken, PA, USA, 2015.

39. Tan, Y.; Li, X.; Wu, J. Internal Influence Factors of Asphalt-Aggregate Filler Interactions Based on Rheological Characteristics. *J. Mater. Civil Eng.* **2012**, *24*, 1520–1528.

40. Zhang, J.; Li, X.; Liu, G.; Pei, J. Effects of material characteristics on asphalt and filler interaction ability. *Int. J. Pavement Eng.* **2017**, 1–10, doi:10.1080/10298436.2017.1366765.

41. Zaniewski, J.P.; Reyes, C.H. *Evaluation of the Effect of Fines on Asphalt Concrete*; Technical Report; West Virginia University: Morgantown, WV, USA, 2003.

42. Muniandy, R.; Aburkaba, E.; Yunus, R.; Hamid, H.; Salihudin, H. Influence of Mineral Filler Particle Size and Type on Rheological and Performance Properties of SMA Asphalt-filler Mastics. *Asian J. Appl. Sci.* **2012**, *5*, 522–537.

43. Wen, H.; Zhang, K.; Hobbs, A.; Edburg, S.L. Microstructural characterization and micromechanics of asphaltic materials–II: Simulation of drying aggregate in asphalt plants. In *Asphalt Pavements*, 2nd ed.; Kim, R.Y., Ed.; CRC Press Taylor & Francis Group: London, UK; New York, NY, USA, 2014; Volume 1, pp. 963–970, ISBN 978-1-138-02693-3.

44. Dukatz, E.L.; Anderson, D.A. The Effect of Various Fillers on the Mechanical Behavior of Asphalt and Asphaltic Concrete. *J. Assoc. Asph. Pavements* **1980**, *49*, 530–549.

45. Naemchan, K.; Meejoo, S.; Onreabroy, W.; Limsuwan, P. Temperature Effect on Chicken Egg Shell Investigated by XRD, TGA, and FTIR. *Adv. Mater. Res.* **2008**, *55–57*, 333–336.

46. Jazie, A.A.; Pramanik, H.; Shinha, A.S.K.; Jazie, A.A. Egg Shell as Eco-friendly Catalyst for Transesterification of Rapeseed Oil: Optimization for Biodiesel Production. *Int. J. Sustain. Dev. Green Econ.* **2013**, *2*, 27–32.

47. Siddiqui, M.N.; Ali, M.F.; Shirokoff, J. Use of X-ray diffraction in assessing the aging pattern of asphalt fractions. *Fuel* **2002**, *81*, 51–58.

48. AlHumaidan, F.S.; Hauser, A.; Rana, M.S.; Lababidi, H.M.S.; Behbehani, M. Changes in asphaltene structure during thermal cracking of residual oils: XRD study. *Fuel* **2015**, *150*, 558–564.

49. Rigo, V.A.; Metin, C.O.; Nguyen, Q.P.; Miranda, C.R. Hydrocarbon Adsorption on Carbonate Mineral Surfaces: A First Principles Study with van der Waals Interactions. *J. Phys. Chem. C* **2012**, *116*, 24538–24548.

50. Wang, H.; Grant, D.J.; Burns, P.C.; Na, C. Infrared Signature of the Cation-π Interaction between Calcite and Aromatic Hydrocarbons. *Langmuir* **2015**, *31*, 5820–5826.

51. Buttlar, W.G.; Bozkurt, D.; Al-Khateeb, G.G.; Waldhoff, A.S. Understanding Asphalt Mastic Behavior through Micromechanics. *Transp. Res. Rec. J. Transp. Res. Board* **1999**, *1681*, 157–169.

52. Al-Qadi, I.; Fini, E.; Elseifi, M.; Masson, J.F.; McGhee, K. Viscosity Determination of Hot-Poured Bituminous Sealants. *Transp. Res. Rec. J. Transp. Res. Board* **2006**, *1958*, 74–81.

53. Al-Qadi, I.L.; Fini, E.H.; Elseifi, M.A.; Masson, J.F.; McGhee, K.M. Development of a Viscosity Specification for Hot-Poured Bituminous Sealants. *J. Test. Eval.* **2007**, *35*, 395–403.

54. Winniford, R.S. The rheology of asphalt-filler systems as shown by the microviscometer. *Am. Soc. Test. Mater.* **1961**, *STP309*, 109–120.

55. Zapién-Castillo, S.; Rivera-Armenta, J.L.; Chávez-Cinco, M.Y.; Salazar-Cruz, B.A.; Mendoza-Martínez, A.M. Physical and rheological properties of asphalt modified with SEBS/montmorillonite nanocomposite. *Constr. Build. Mater.* **2016**, *106*, 349–356.

56. Shafabakhsh, G.H.; Ani, O.J. Experimental investigation of effect of Nano TiO2/SiO2 modified bitumen on the rutting and fatigue performance of asphalt mixtures containing steel slag aggregates. *Constr. Build. Mater.* **2015**, *98*, 692–702.

57. Nciri, N.; Kim, J.; Kim, N.; Cho, N. An In-Depth Investigation into the Physicochemical, Thermal, Microstructural, and Rheological Properties of Petroleum and Natural Asphalts. *Materials* **2016**, *9*, 859, doi:10.3390/ma9100859.

58. Asociación Española de Normalización y Certificación (AENOR). *UNE-EN 13043, Aggregates for Bituminous Mixtures and Surface Treatments for Roads, Airfields and Other Trafficked Areas*; Asociación Española de Normalización y Certificación (AENOR): Madrid, Spain, 2004. (In Spanish)

59. Jahromi, S.G. Estimation of resistance to moisture destruction in asphalt mixtures. *Constr. Build. Mater.* **2009**, *23*, 2324–2331.

60. Woszuk, A.; Zofka, A.; Bandura, L.; Franus, W. Effect of zeolite properties on asphalt foaming. *Constr. Build. Mater.* **2017**, *139*, 247–255.

61. Woszuk, A.; Franus, W. A Review of the Application of Zeolite Materials in Warm Mix Asphalt Technologies. *Appl. Sci-Basel* **2017**, *7*, 293, doi:10.3390/app7030293

62. Zhang, Y.; Leng, Z.; Zou, F.; Wang, L.; Chen, S.S.; Tsang, D.C.W. Synthesis of zeolite A using sewage sludge ash for application in warm mix asphalt. *J. Clean. Prod.* **2018**, *172*, 686–695.

63. Oner, J.; Sengoz, B. Utilization of Recycled Asphalt Concrete with Warm Mix Asphalt and Cost-Benefit Analysis. *PLoS ONE* **2015**, *10*, e116180, doi:10.1371/journal.pone.0116180.

64. Masson, J.F.; Polomark, G.; Collins, P. Glass transitions and amorphous phases in SBS–bitumen blends. *Thermochim. Acta* **2005**, *436*, 96–100.

65. Nciri, N.; Kim, N.; Cho, N. New insights into the effects of styrene-butadiene-styrene polymer modifier on the structure, properties, and performance of asphalt binder: The case of AP-5 asphalt and solvent deasphalting pitch. *Mater. Chem. Phys.* **2017**, *193*, 477–495.

66. Clopotel, C.; Bahia, H. The effect of bitumen polar groups adsorption on mastics properties at low temperatures. *Road Mater. Pavement* **2013**, *14*, 38–51.

67. Guo, M.; Tan, Y.Q.; Zhang, L. Effect of Filler on Glass Transition of Asphalt Mastics. *Adv. Eng. Forum* **2012**, *5*, 376–381.

68. Tan, Y.; Guo, M. Study on the phase behavior of asphalt mastic. *Constr. Build. Mater.* **2013**, *47*, 311–317.